IEEE Open Journal of
Power Electronics

Received 13 March 2023; accepted 20 April 2023. Date of publication 25 April 2023;
date of current version 30 June 2023. The review of this paper was arranged by Associate Editor Yingyi Yan.

Digital Object Identifier 10.1109/OJPEL.2023.3270374

Responsive and Resilient Vector Current Control for Variable Grids

MATHIEU KERVYN DE MEERENDRE, KHALED H. AHMED (Senior Member, IEEE), AND AGUSTÍ EGEA-ÀLVAREZ (Member, IEEE)

Electrical and Electronic Engineering Department, University of Strathclyde, G1 1XW Glasgow, U.K.

CORRESPONDING AUTHOR: MATHIEU KERVYN DE MEERENDRE (e-mail: mathieu.kervyn@strath.ac.uk

The work of Agustí Egea-Àlvarez was supported by the Royal Academy of Engineering through the Industrial Fellowships program, under Grant IF223-169. This work was supported in part by the Engineering and Physical Sciences Research Council, and in part by the National Productivity Investment Fund, under Grant EP/R512205/1.

ABSTRACT This article presents a set of control enhancements for standard vector current control (VCC) that improves its stability and dynamic performance in an extended range of SCRs. Increasingly, the local SCR as seen by the converter fluctuates, making it difficult to tune the control algorithms. Usually, stability is prioritised over performance and converters become less responsive. The modifications proposed in this article allow VCC to maintain high dynamic performance and stability, optimised to the real-time grid conditions. These modifications do not alter the standard operation of the outer loops, the current controller or the phase-locked loop. Instead, a Pre-emptive Voltage Decoupler (PVD) is introduced to compensate reactive current for changes in active current, thus decoupling the local voltage from active power. The PVD is optimised to the grid conditions by an impedance estimator. Further, an instability detector is proposed, anticipating instability and triggering preventive action, improving the resiliency of the converter. Supervisory control is employed to coordinate instability detection, prevention, impedance estimation and PVD optimisation. As a result, VCC is more responsive and adaptable to variable grid conditions. It is also more resilient to grid events, such as the loss of a transmission line.

INDEX TERMS Active power, voltage decoupling, impedance estimation, instability detection, vector control, weak grid.

I. INTRODUCTION

Carbon reduction ambitions [1] coupled with the reducing costs of low carbon electricity [2], has led to an increase in converter interfaced infrastructure [3]. However, integrating large amounts of converter-based renewables into the electrical network presents new challenges. This includes difficulty in balancing demand and generation, reduced system inertia and reduced voltage stiffness in networks [4]. This article focuses on the control of power converters in networks with variable voltage stiffness, including weak grids.

The majority of grid-connected voltage source converters (VSCs) currently installed use vector current control (VCC) [5], which over the years has accumulated a substantial amount of academic and industrial experience. VCC synchronises to the point of common coupling (PCC) voltage via a phase-locked loop (PLL) to control active and reactive power independently [6]. In a stiff grid, the PCC voltage is mostly constant and unaffected by variations in active power, allowing stable operation [7]. However, in weak grids, the stiffness of the PCC voltage is reduced [8], necessitating converters to provide reactive power support to facilitate active power transfer [9]. In the context of this article, a very weak grid is when the short circuit ratio (SCR) is below 2 and a weak grid is when the SCR is between 2 and 3 [10].

Further complicating the application of voltage support is the fact that real grids experience varying SCR conditions [11], [12]. A sudden change in SCR in an already weak network is arguably a contributing factor to the 9 August 2019 power outage. The technical report [13] describes how the local network at the Hornsea wind farm was already weak and experiencing oscillatory behaviour when a transmission line (the Eaton Socon – Wymondley 400 kV circuit) was

disconnected due to a lightening stike. It can be inferred that the transmission line loss further reduced Hornsea wind farm's local grid strength, increasing the coupling between active and reactive power. Such conditions could result in undamped oscillations and for the wind farm's protection systems to trip.

In the literature, there are two main approaches to improving VCC stability in weak grids. The first is to make the controller stable across all operating regions with *stationary control parameters*. The second approach is to use *adaptive control parameters*, allowing the controller to respond to evolving grid conditions. This research is reviewed in the context of controller dynamics, transient stability and inherent current limiting capabilities of VCC.

Stationary control parameter literature tend to propose modifications to the current controller, the PLL, or the outer loop of VCC. In the case of current controller modification, [14] introduces a magnitude and phase compensation branch to the output of the current controller. However, by bypassing the current controller gains, the inherent current limiting capabilities of VCC are compromised.

With regards to PLL modification, [15] proposes to synchronise to an artificial voltage through the use of virtual impedance. However, this results in larger PCC voltage fluctuations. Various other arrangements of virtual impedances within the PLL are proposed [16], [17], [18], [19], but as explained in [20], many of these achieve improved stability through reduced PLL bandwidth. It is unclear how well such modifications perform in strong grids. As an alternative, [20] proposes a feed-forward branch that bypasses the current controller to offset PLL-induced disturbances. However, this is far from ideal as the VCC's overcurrent protection capabilities become compromised, similarly to [14].

Alternatively, stability in weak grids can be improved by feed-forwarding a voltage signal to the reactive current reference for reactive support purposes [21], [22], [23]. These papers follow a similar pattern: take the voltage signal (or one derived from voltage measurements), process it through a transfer function, and add it to the reactive current reference. However, the voltage support is reactionary as it can only respond to existing voltage disturbances. Thus, while these proposals may improve the stability of the converter, their ability to improve the dynamic performance of VCC is limited. An improvement to voltage feed-forward is presented in [24], which employs a gain-scheduled multi-variable controller designed for high-bandwidth control in very weak grids. Similarly, [25] uses a feed-forward branch that considers both active power reference and voltage measurement. Both [24], [25] show promise because they attempt to predict the required reactive support, rather than react to voltage measurements. However, they also have drawbacks; [24] is highly optimised (and therefore limited) to a SCR of 1, which is impractical. [25] is sensitive to the tuning of the active power loop as the power reference is processed by both the feed-forward element and the active power loop simultaneously. It also does not address the implications of large SCR variations.

To summarise, the range of stable control parameters when using stationary parameters in very weak grids is narrow and not particularly dynamic [26]. In effect, dynamic performance is reduced in favour of stability.

Adaptive control parameters is the second approach to improving VCC stability, which can determine the real-time grid conditions and respond to them appropriately. This information is then used to tune the current controller, the outer loop, the PLL, or a combination.

For current controllers in VCC, [27], [28] propose real time tuning via grid impedance estimates. In [27], the current controller proportional and integral gains are re-calculated for every inductance estimation such that the undamped natural frequency and damping ratio of the current controller remains constant. In [28], the estimated line inductance similarly affect the overall current controller gains. Additionally, [28] also uses the inductance estimates to estimate the stiff grid voltage and feed this forward to the reactive current reference for reactionary reactive support (similar to [21], [22], [23]). However, the converter response to power reference changes appears slow, with the objectives set on stability only. Transient stability is tested by stepping up the grid strength from a very weak grid to a strong grid (SCR step change from 0.96 to 4.8). This is not representative of the most problematic grid events, such the loss of a transmission line, where system is required to settle at reduced voltage stiffness. Adaptive techniques are not limited to VCC current controllers, with [29] proposing to adaptively tune a proportional resonant (PR) current controller. However, the exact implementation into adaptive control is unclear, with no equations or block diagrams.

With regards to PLL adaptation, [30] directly modifies the PLL bandwidth depending on the grid impedance estimation, reducing the controller bandwidth proportionally with the grid impedance. Another article [31], suggests synchronising to the voltage frequency instead of the voltage angle. The main concern in the article is the loss of synchronisation during large fault scenarios, but it is unclear how this affects the stability and dynamic capabilities of the converter in variable SCR conditions.

With the exception of [15], [28], most of the literature does not consider large signal stability due to disruptive grid events. As explained earlier, the loss of a transmission line can cause significant disruption, thus resiliency to such events should be considered in converter control literature.

The aim of this article is to propose a controller that performs well in realistic and variable grid conditions, while remaining compatible with existing VCC controlled VSCs. These objectives are as follows:

1) The proposed controller must be based on classical VCC with standard PLL, current controller and outer loop. These limitations will facilitate retrofitting existing converters. The current limiting capabilities of VCC cannot be compromised.
2) Demonstrate small-signal stability at high power outputs independently of SCR but especially for weak grids.

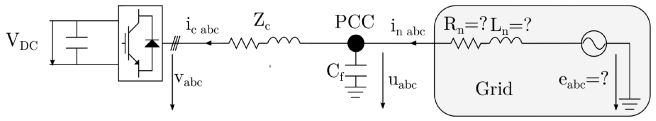

FIGURE 1. System under study.

3) Maintain VCC dynamic capabilities independently of SCR. For this objective, a numerical target can be set based on [26], which proposes a target settling time of < 750 ms to a step in power. Similarly, a target rise time for the power controller is set at < 40 ms and a target settling time is set to $<$ 400 ms. These objectives are assessed using experimental data.
4) Demonstrate resiliency to grid events which result in sudden SCR changes. This objective will be demonstrated experimentally by subjecting the converter to a large increase in impedance, resulting in a weak grid suddenly becoming very weak.

The coordinated control enhancements proposed in this article enable VCC to adapt to varying non-linear grid conditions without any additional sensors, complex gain-scheduling or unusual synchonisation mechanisms, thus achieving objective 1. Objective 2 is met with the proposed novel pre-emptive voltage decoupler. This mechanism is optimised for varying grid conditions through an impedance estimator, thus enabling good dynamic performance across all SCRs and realising objective 3. Objective 4 is attained by combining a novel instability detector with a power reduction mechanism. This is in itself a novel concept – there are no proposals in the existing literature to prevent the interruption of converter operation during significant grid events, with any instability much more likely to trip protection systems.

II. SYSTEM UNDER STUDY

A schematic of the power system is presented in Fig. 1. The grid impedances selected reflect a wide range of SCRs, including very weak, weak and strong conditions. Given the available laboratory equipment constraints, the resulting SCR values are 1.38, 2.77 and 5.53. The grid parameters are presented in Appendix B.

In Fig. 1, v_{abc} is the converter voltage, $i_{c\,abc}$ is the converter current, u_{abc} is the PCC voltage, $i_{n\,abc}$ is the grid current and e_{abc} is the grid voltage. V_{DC} is the dc-link voltage. The voltages are also presented as phasors relative to the PCC voltage angle, such that $\overline{U} = U\angle 0$ and $\overline{E} = E\angle\delta$. With regards to the passive components, R_c, L_c and C_f are the resistance, inductance and capacitance of the converter filter, R_n and L_n are the grid resistance and inductance. Combined, R_n and L_n form the grid impedance, $\overline{Z}_n$, where $\overline{Z}_n = R_n + j\omega L_n = R_n + jX_n$. In phase form, $\overline{Z}_n = Z_n\angle\phi$. In this article, all impedance values are Thévenin equivalent impedances (i.e. at the fundamental frequency ω) unless otherwise specified. In a weak grid, this is a common assumption as the large grid impedance can be acceptably represented using the Thévenin equivalent values, similarly to [32], [33].

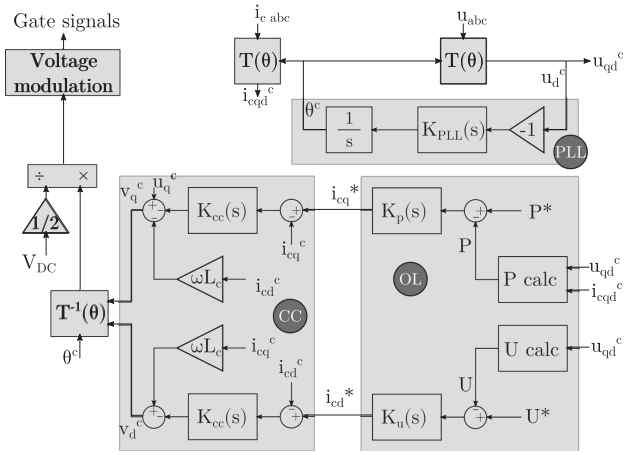

FIGURE 2. Classical VCC schematic.

Network stiffness is usually described with the SCR. It is calculated as [18], [34]

$$SCR = \frac{S_{SC}}{S_{rated}} = \frac{\frac{E_{ll}^2}{Z_n}}{S_{rated}} \tag{1}$$

where S_{SC} is the network power when a three-phase balanced short circuit occurs, S_{rated} is the converter rating, and E_{ll} is the line-to-line grid voltage. Given the high X_n/R_n ratios experienced in transmission networks, Z_n is often substituted with X_n.

III. CLASSICAL VCC

Classical VCC, without modifications, employs an outer loop (OL), a current controller (CC), a phase-locked loop (PLL) and Park transforms (T(θ)). The overall layout of VCC is presented in Fig. 2.

Where i^c_{cqd} and u^c_{qd} are the converter current and the PCC voltage in the qd-frame. The superscript c refers to the converter frame, to differentiate the converter-frame variables from the grid-frame variables. θ^c is the synchonisation angle. P and U are the active power and voltage magnitude. The asterix superscript refers to reference signals.

The Park transformation is implemented such that the real component (q) is aligned with the positive real axis and the imaginary component (d) is lagging by 90°, such that $\overline{U} = u_q - ju_d$.

The role of the PLL is to synchronise the rotating (qd) reference frame to the PCC voltage, such that

$$\frac{\theta^c}{u_d} = -\frac{K_{PLL}(s)}{s} \tag{2}$$

where $K_{PLL}(s)$ is a proportional-integral (PI) controller. The proportional and integral gains are determined by the desired damping ratio ζ and bandwidth ω_{PLL}, such that the proportional gain $K_{PLL\,p} = \frac{2\zeta\omega_{PLL}}{U_{peak}}$ and the integral gain $K_{PLL\,i} = \frac{\omega^2_{PLL}}{U_{peak}}$ [35].

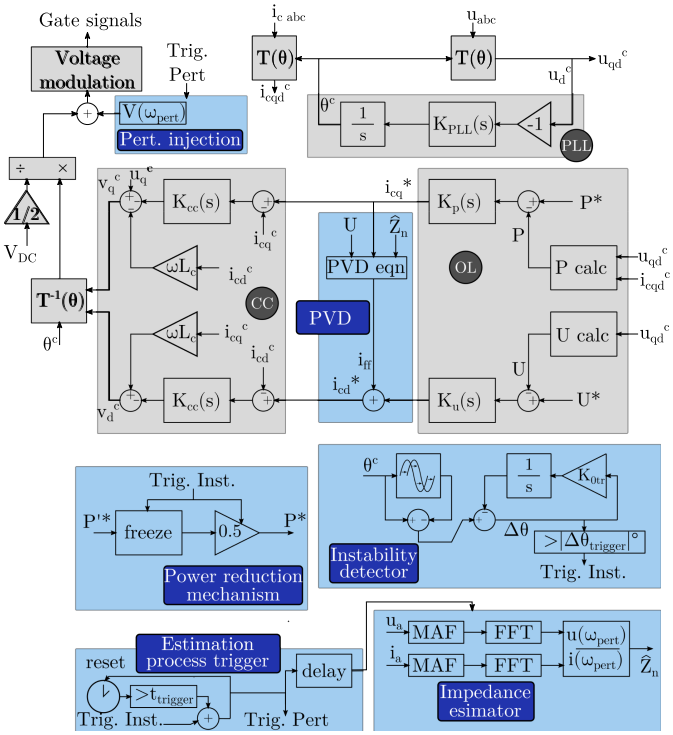

FIGURE 3. Proposed control schematic.

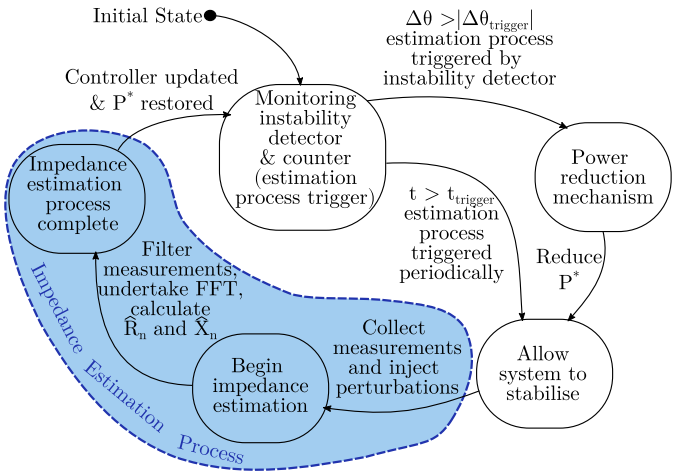

FIGURE 4. State machine representation of supervisory control, used to coordinate the proposed modifications to VCC.

The current loop can be defined as

$$v_q = u_q - i_{cd} L_c \omega - K_{CC}(s)(i^*_{cq} - i_{cq}) \tag{3}$$

$$v_d = u_d + i_{cq} L_c \omega - K_{CC}(s)(i^*_{cd} - i_{cd}) \tag{4}$$

where $K_{CC}(s)$ are PI controllers.

The outer loop is responsible for active power and voltage magnitude control via PI controllers $K_P(s)$ and $K_U(s)$. The calculation of power and voltage is as follows: $P = \frac{3}{2}(i^c_{cq} u^c_q + i^c_{cd} u^c_d)$ and $U = \sqrt{u^c_q + u^c_d}$.

The control parameters employed in this work are presented in Appendix B. For more detail on classical VCC, please refer to [6], [35].

IV. PROPOSED MODIFICATIONS TO VCC

The proposed controller modifications are presented in blue in Fig. 3 in relation to the classical control components described in Section III.

From the top left to the bottom right of the figure, the modifications to the control are as follows:

- The impedance estimator requires a steady state perturbation. This is done by $V(\omega_{pert})$ in the perturbation injection block.
- The Pre-emptive Voltage Decoupler (PVD) compensates the reactive current reference i^*_{cd} for changes in active current reference i^*_{cq}, PCC voltage U, and estimated grid impedance $\hat{Z}_n$.
- The power reduction mechanism reduces the power reference seen by the outer loop if the instability detector is triggered. To differentiate between the uncompensated and compensated power references, the uncompensated power reference is denoted with a dash, P'^*.
- The instability detector monitors the evolution of the reference angle over a pre-determined time period. It tracks zero during normal operation due to the low bandwidth integral gain, K_{0tr}.
- For the purposes of real-time monitoring of grid impedance, an estimation process trigger periodically launches the impedance estimator. $t_{trigger}$ is the duration of the period.
- The impedance estimator draws on perturbed voltage and current measurements $u(\omega_{pert})$ and $i(\omega_{pert})$ to produce an impedance estimation. MAF refers to moving average filter and FFT refers to Fast Fourier Transform.

The coordination of these tasks is performed by the high level supervisory control, described using state machine notation in Fig. 4.

The starting point of the state machine is the monitoring of instability detection and periodic counter. If the instability detector is triggered, the power reduction mechanism reacts and the system is allowed to stabilise at a reduced power reference, at which it will remain until the end of the estimation process. If the periodic counter is triggered, the current power reference is held until the end of the estimation process. The impedance estimation process then begins, with the perturbation injection, measurement filtering, and impedance calculation. The power reference is then recovered and normal operation is resumed.

A. IMPEDANCE ESTIMATION

In previous work, the authors have reviewed and categorised local impedance estimation techniques [36]. Due to its simplicity, accuracy and on-demand estimation capabilities, the

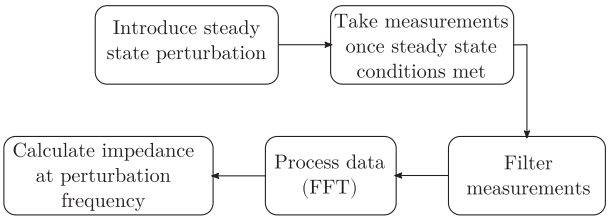

FIGURE 5. Impedance estimation process.

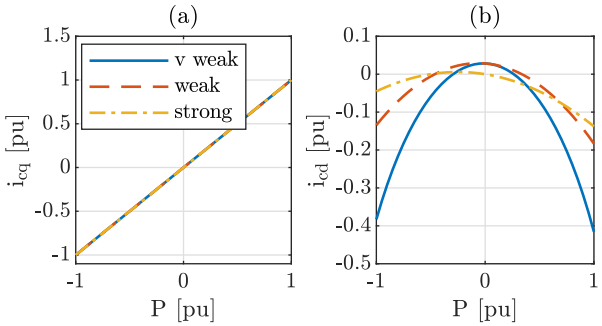

FIGURE 6. (a) Steady state relationship between active power and active current and (b) steady state relationship between active power and reactive current, for SCRs of 1.38, 2.77 and 5.53.

nonharmonic sinusoidal estimator is used in this article. The main drawback is the total time required for the estimation process, because it is necessary to allow the system to stabilise before introducing any perturbations. It is based on [37] and described in Fig. 5.

The estimation process introduces a low magnitude nonharmonic steady state voltage perturbation (Fig. 3). The perturbation frequency is chosen such that it is near the fundamental to avoid error due to nonlinearities; in this article 75 Hz is used, as suggested in [37]. Once the system has settled, the impedance estimator process begins. The voltage and current measurements in phase A are filtered with a moving average filter, and then the perturbation frequency components are extracted using the Fourier transform.

$$\overline{U}(\omega_p) = \int_{-T_{est}}^{0} u_a(t) e^{j\omega_p t} dt \tag{5}$$

$$\overline{I}(\omega_p) = \int_{-T_{est}}^{0} i_a(t) e^{j\omega_p t} dt \tag{6}$$

where T_{est} is the estimation period and ω_p is the perturbation frequency. The impedance is then calculated

$$\hat{\overline{Z}}_n(\omega_p) = \hat{R}_n(\omega_p) + j\hat{X}_n(\omega_p) = \frac{\overline{U}(\omega_p)}{\overline{I}(\omega_p)} \tag{7}$$

The voltage perturbation employed is 0.005% of the magnitude of the PCC voltage, thus the perturbation is very small, minimising the disruption to the network. Small perturbations are one of the advantages of such steady state techniques, especially when compared to impulse-response estimators [36]. The size of the perturbation must be carefully chosen to give accurate impedance estimations for a wide range of grid conditions: too big, and the settling time will be increased; too small, and the response will be too small to measure accurately. For the same reasons, [37], [38] also use steady state impedance estimators with small perturbations.

B. PRE-EMPTIVE VOLTAGE DECOUPLER

The control blocks discussed in this section are inserted between the outer loop and the current controller, as per Fig. 3. In a strong grid, the relationship between active power and active current is linear for all power level outputs, as per Fig. 6(a). However, this is not the case for active power and reactive current as demonstrated in Fig. 6(b). The weaker the grid, the more coupled active power and voltage become [39]. This coupling is due to the increased reactive power injection required to support the PCC voltage.

Many of the previously discussed papers [21], [22], [23], [28] address weak grid instability through a voltage feed-forward mechanism, reacting to P-U coupling by compensating for changes in voltage measurement. An improvement to this compensation mechanism would be to pre-empt how the voltage changes in real-time before it actually changes, by using additional information such as the active current reference and the grid impedance. This would compensate reactive current for changes in active current. Such a mechanism is derived here: consider the apparent power equation $\overline{S} = 3\overline{U}(\overline{I}_n^{conj})$ and Kirchoff's Voltage Law $\overline{I}_n = \frac{\overline{E}-\overline{U}}{\overline{Z}_n}$

$$P = \frac{3U(EX_n \sin(\delta) + R_n(E\cos(\delta) - U)}{X_n^2 + R_n^2} \tag{8}$$

$$Q = \frac{3U(X_n(E\cos(\delta) - U) - ER_n \sin(\delta))}{X_n^2 + R_n^2} \tag{9}$$

Given that $i_{nq} = P/3\,U$ and that $i_{nd} = Q/3\,U$, and assuming that $E \equiv U$

$$i_{nq} = \frac{UX_n \sin(\delta) + R_n(U\cos(\delta) - U)}{X_n^2 + R_n^2} \tag{10}$$

$$i_{nd} = \frac{X_n(U\cos(\delta) - U) - R_n U \sin(\delta)}{X_n^2 + R_n^2} \tag{11}$$

By considering the trigonometric function

$$A\sin(x) + B\cos(x) = \sqrt{A^2 + B^2}\,\sin\left(x + a\tan\left(\frac{B}{A}\right)\right) \tag{12}$$

and taking into account the current at the filter capacitor, $\overline{I}_{cap}$, such that $\overline{I}_c = \overline{I}_n + \overline{I}_{cap}$, (10) and (11) can be solved for i_{cd}. Thus, i_{cd} is a function of i_{cq}, U and Z_n. This can be adapted such that i_{cd}^* is compensated for changes in i_{cq}^*, U and $\hat{\overline{Z}}_n$. This compensation term is described as the feed-forward current, i_{ff}, presented below in (13) and implemented in the PVD, as

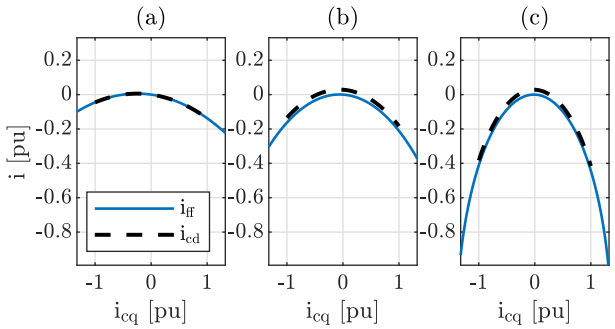

FIGURE 7. Relationship between active and reactive current comparing steady state values and feed-forward values for (a) SCR = 5.53, (b) SCR = 2.77 and (c) SCR = 1.38.

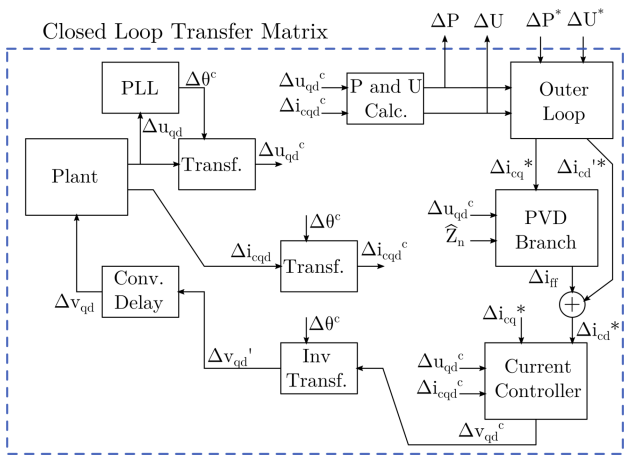

FIGURE 8. Closed system transfer matrix: Representation of small-signal closed-loop system.

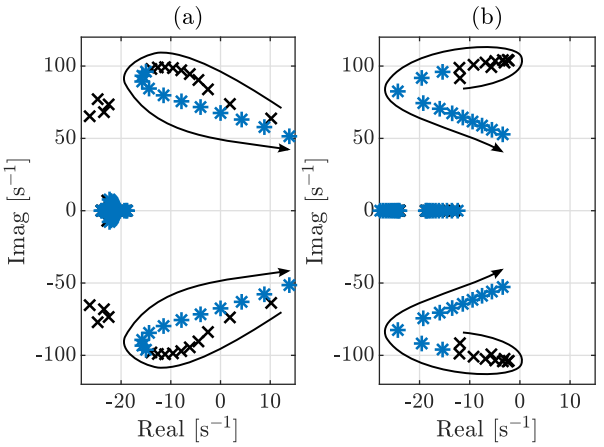

FIGURE 9. Eigenvalues of linear system, (a) without the PVD and (b) with the PVD for $P = -1$ to $P = 1$ pu in steps of 0.1 pu.

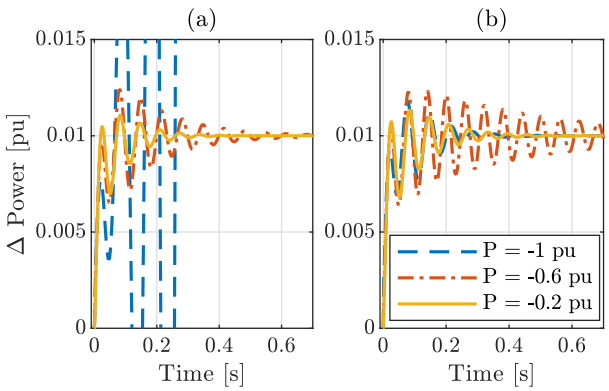

FIGURE 10. Response to a step in power (a) without the PVD and (b) with the PVD, in a very weak grid.

per Fig. 3 (i.e. i_{ff} is added to i^*_{cd}).

$$i_{ff} = \frac{-U\hat{X}_n \pm U\hat{Z}_n\sqrt{1 - \frac{(\hat{R}_n U + i^*_{cq}(\hat{X}_n{}^2 + \hat{R}_n{}^2))^2}{U^2\hat{Z}_n{}^2}}}{\hat{R}_n{}^2 + \hat{X}_n{}^2} + \frac{U}{X_c} \quad (13)$$

where X_c is the capacitor reactance. To validate (13), the calculated i_{ff} is compared to the linearised values of i_{cd} in Fig. 7, for three different SCRs.

The similarity of i_{ff} and i_{cd} in Fig. 7 demonstrates the potential for (13) to decouple the reactive loop from the active loop in the controller by pre-emptively compensating i^*_{cd} for changes in i^*_{cq}, and thus active power reference.

The closed system transfer matrix, based on [26], [40], is used as the foundation for the small-signal studies. The matrix is composed of linearised equations for the Plant (electrical systems), PLL, transforms, current controller, outer loop, delays and PVD. This is presented graphically in Fig. 8.

The closed system transfer matrix is used in Fig. 9 to compare the eigenvalues of two systems: with and without the PVD, linearised for a range of power levels from $P = -1$ to 1 pu in increments of 0.1 pu. The values for $P < 0$ pu are in black crosses, and the values for $P \geq 0$ pu are in blue asterisks.

Given that all real negative eigenvalues are stable, and all real positive eigenvalues are unstable, the location of the eigenvalues in Fig. 9 demonstrate vastly improved steady state stability with the PVD. With no PVD, instability sets in for $P \leq -0.8$ pu and $P \geq 0.7$ pu. With the PVD, there are no right hand eigenvalues at any operating point. However, this does come at a trade-off at $P \approx -0.6$ pu where eigenvalues come close to the right hand plane. As this happens at relatively large imaginary numbers, these eigenvalues are likely to be oscillatory.

The next consideration is the steady state response to changes in power reference with and without the PVD, for a SCR of 1.38, as per Fig. 10. This figure demonstrates the increased range in step response, but also the oscillatory nature of the response. Notice the increased oscillation at $P = -0.6$ pu in red, due to the location of the eigenvalues at that power level. This is deemed to be an acceptable trade-off for the increased small-signal stability at other power levels.

In summary – the small-signal analysis demonstrates a clear improvement with the PVD. The unstable eigenvalues become stable, and the small-signal steps demonstrate good response to changes in power reference.

C. INSTABILITY DETECTOR AND POWER REDUCTION MECHANISM

A major grid event, such as the loss of a transmission line, can result in instability despite the improved small-signal stability of the PVD. To avoid this, it is suggested to monitor changes in the PCC voltage angle θ^c as a proxy for the voltage angle δ (the angle of the stiff grid voltage relative to the PCC voltage), which is not available with local measurements only. In an inductive grid, δ is proportional to active power, given $P = \frac{EU}{X_n}\sin(\delta)$ [41]. Thus, to avoid the voltage angle runaway that leads to instability, it is recommended to reduce the active power reference when instability is suspected.

The proposed instability detector monitors $\Delta\theta$, which compares the angle θ^c with the delayed angle (θ^c_D), such that $\Delta\theta = \theta^c - \theta^c_D$. In normal conditions, the output of the detection mechanism might be a constant non-zero value. To allow for a triggering mechanism, a zero tracking mechanism is implemented so that $\Delta\theta$ is zero in normal operation, also included in the Fig. 3 schematic. The zero tracking mechanism has a low bandwidth, bearing no impact on the functionality of the instability detection. The trigger point and the delay, presented in Appendix B, are optimised for quick response and appropriate sensitivity.

Once triggered, the instability detector reduces the power reference. This enables the system to settle and the supervisory control to re-optimise the PVD with a new impedance estimation, thus providing a resilient response to disruptive grid events. The performance of the instability detector and power reduction mechanism is simulated in a case study in Fig. 11, where the SCR changes from 2.77 to 1.38 at 0.1 s while the converter is injecting 0.8 pu of power into the grid. For demonstration purposes, the outer loop gains in this case study are multiplied by a factor of 7. This reduces the stability margins and accentuates the oscillations.

In the case study, the rapid nature of the controller combined with the high grid impedance causes the converter to become oscillatory. Without the instability detector and a reduction in power output, the step change in impedance causes a resonance to build in the system, as demonstrated by the orange trace. However, by tracking $\Delta\theta$ and halving the power reference when the grid event is detected, it is possible to prevent oscillations from building (blue trace). In this simulation, the change in grid impedance is almost immediately detected and triggers a reduction in power reference. The reference is then recovered at 0.65 s with a new impedance estimation. For clarity, time-frames in this example are not representative of the final implementation, but merely for demonstration purposes.

The relationship between P and δ is dependent on SCR, with low SCRs demanding a higher δ for the same amount of active power transfer. This can be visualised most clearly

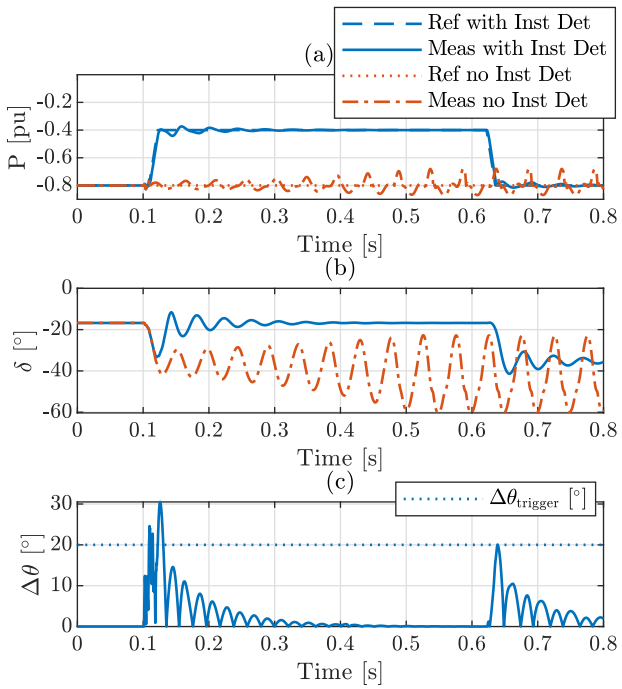

FIGURE 11. Simulation of step change in grid impedance with time-domain plots of (a) power, (b) voltage angle and (c) monitored angular change.

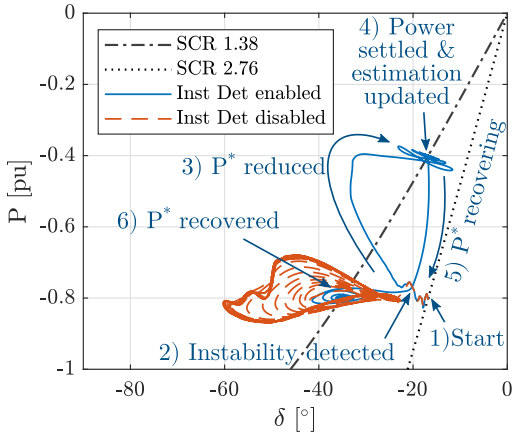

FIGURE 12. Effect of SCR on voltage angle, in inverting mode.

by plotting δ against P, as per Fig. 12, for SCRs of 1.38 and 2.77. In this figure, both scenarios with and without instability detection (from Fig. 11) are reproduced to highlight how the reduction in active power, and thus voltage angle, helps the converter recover from a disruptive grid event.

For completeness, this detection mechanism is different to vector shift (VS) protection, which is used to detect loss of mains [42]. VS is determined by calculating the zero-crossing times between the present and previous cycle, using half cycle measurements. The relay will trip is 5 of the 6 results (2 per phase) are above the threshold. The proposed instability

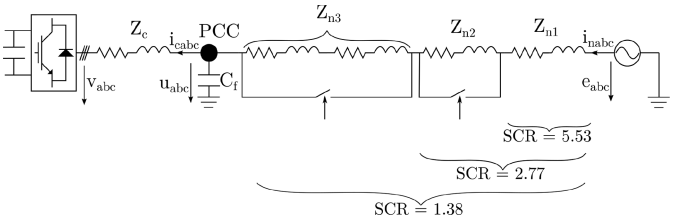

FIGURE 13. Schematic of test rig.

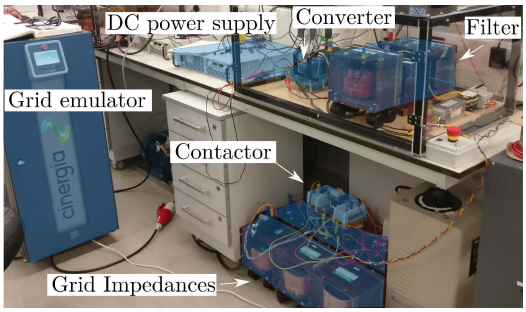

FIGURE 14. Photograph of test rig.

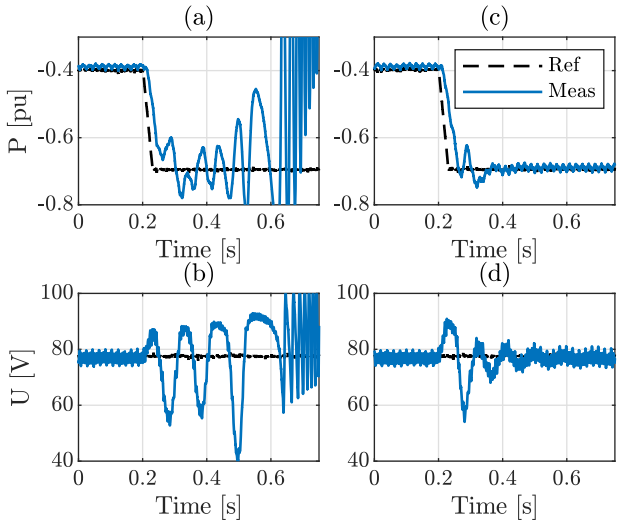

FIGURE 15. Step change in power for both VCC without a PVD (a) and (b), and with a PVD (c) and (d).

detector uses the integration of 50 frequency samples over 10 ms (given $f_{sampling} = 5$ kHz) to obtain $\Delta\theta$.

V. METHODS AND PROCEDURES

The proposed controller is implemented into an Texas Instruments F28379D ControlCard attached to a 1 kW SiC MOSFET two-level converter. The grid is emulated using a Cinergia grid emulator and the stiffness is arranged via 3 different impedances and contactors. A schematic of the hardware used for the experimental set-up is presented in Fig. 13 and a photograph is presented in Fig. 14. The PWM filter is represented by a capacitor (C_f).

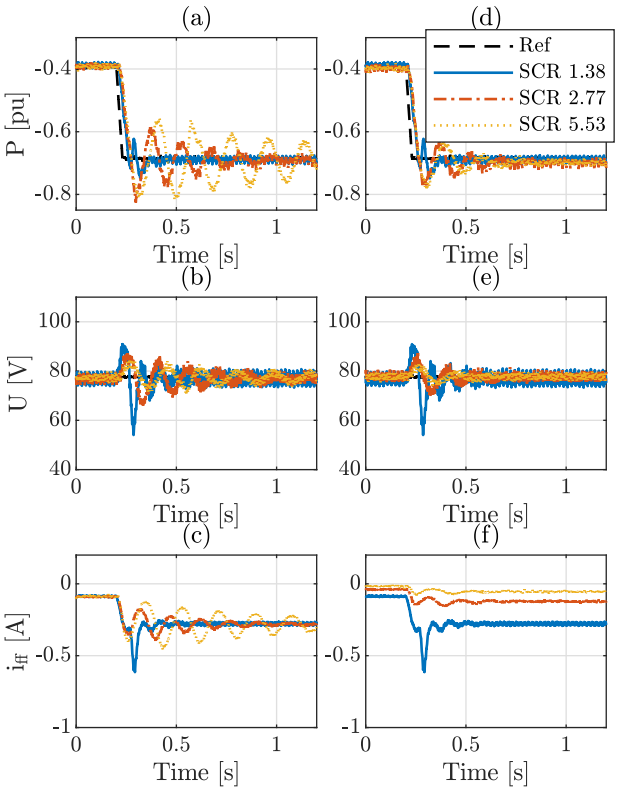

FIGURE 16. Step change in power for various SCRs with fixed tuning at SCR = 1.38 (a)–(c), and correct PVD tuning (d)–(f).

The reliability, performance and robustness of the proposed controller is tested through the following tests:

1) Compare the proposed PVD to a classical VCC without the PVD in a weak grid.
2) Test the PVD for a range of SCRs, with both optimised and unoptimised grid parameters.
3) Test the performance of the converter controller when a large SCR variation occurs.

VI. RESULTS

A. STEP CHANGE IN POWER WITH AND WITHOUT PVD IN A WEAK GRID

The first experiment compares the response to a step in power reference in a very weak network (SCR = 1.38), both with and without the PVD. The power reference step is chosen from −0.4 to −0.7 pu because this is a step representative of a wind turbine capturing a large gust, as well as producing a clear demonstration of the propagating instability when the PVD is disabled. The change in power reference occurs at time instant $t = 0.2$ s. Fig. 15(a) and (b) displays the reference/measured power and voltage signals respectively, without the PVD activated. Fig. 15(c) and (d) displays the same information, but with the PVD activated.

This test demonstrates that, in a very weak grid, the performance of the converter is greatly improved with the PVD. There is some transient behaviour with the PVD, but stability

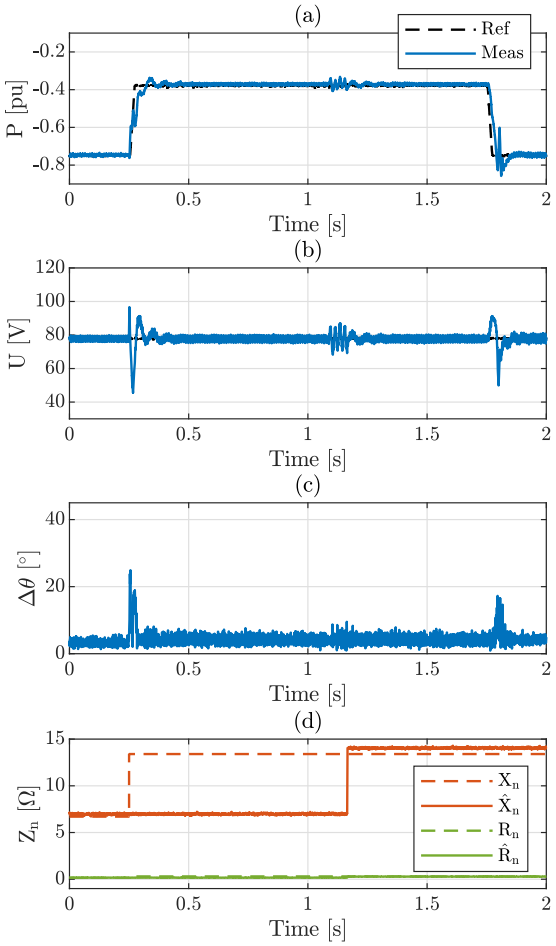

FIGURE 17. Step change in SCR for proposed controller with instability detector and impedance estimator enabled; (a) power, (b) voltage, (c) $\Delta\theta$, and (d) actual impedance and estimated impedance.

is maintained. Without the PVD, the power and voltage controllers fight each other and the resulting oscillations become unstable.

Further, it is possible to extract the rise time and settling time information for this step change in power reference. 10% of the step is reached at 0.207 s and 90% of the step is reached at 0.247 s, resulting in a rise time of 40 ms. With regards to the settling time, a peak value of -0.75 pu is reached at 0.308 s, and the system settles by 0.4 s, resulting in a settling time of < 100 ms. Both values are within the desired dynamic performance.

B. STEP CHANGE IN POWER FOR VARIOUS SCRS FOR OPTIMISED AND NOT OPTIMISED PVD

The second experiment tests the robustness of the PVD in case there is no estimator and compares this to the proposed technique of employing an impedance estimator in conjunction with the PVD. Similarly to Section VI-A, the power is stepped from -0.4 to -0.7 pu at time instant t $= 0.2$ s, repeated for three different SCRs (1.38, 2.77 and 5.53). Fig. 16 presents (a) the power, (b) the voltage and (c) the feed-forward current, with the PVD always assuming worst case scenario (SCR $= 1.38$). The same tests are repeated for Fig. 16(d)–(f) except that the PVD is tuned to the actual grid conditions.

From Fig. 16(a)–(c), it can be determined that incorrect impedance estimation does not necessarily result in instability, but it will impact on the performance of the converter when the grid impedance assumption is sufficiently incorrect. Compare this to (d)–(f), where the correct impedance value is known, improving the response across all grid conditions. This is because the appropriate feed-forward current is produces the appropriate decoupling of P and U, as per Fig. 16(f).

C. STEP CHANGE IN GRID IMPEDANCE WITH INSTABILITY DETECTOR

This experiment tests the coordination of the proposed modifications. A step change in impedance is introduced to emulate the loss of a transmission line, resulting in a drop in SCR from 2.77 to 1.38. The results are presented in Fig. 17 where (a) is the power plot, (b) is the voltage plot, (c) is the $\Delta\theta$ plot and (d) is the actual and estimated impedance. At t $= 0.25$ s, the step change in impedance results in an almost immediate trigger of the power reference due to triggering by the instability detector. Without this reduction in power and the ability to settle at a lower power level, the system becomes unstable. At around 1.2 s, the impedance estimation is undertaken and the PVD is updated. About one second later, the power reference is recovered, and the converter returns to normal operation with an optimised PVD. This test demonstrates converter resilience to unexpected grid events.

VII. CONCLUSION

This article has proposed an enhanced VCC designed for improved dynamic performance in weak grids, adaptability to varying grid conditions and resilience to unexpected grid events. Four different elements are added to the classical VCC: a PVD, an impedance estimator, a instability detector and a power reduction mechanism, all of which are managed by supervisory control. The PVD compensates reactive power for changes in active power reference in low SCRs, the impedance estimator optimises the PVD for the real-time SCR and the instability detector helps to maintain stability when large disturbances occur. In such an event, the power reference is reduced and the PVD re-optimised. The system is robust to incorrect impedance information, but real-time optimisation is recommended.

APPENDIX A
SMALL-SIGNAL MODEL

The following equations represent the electrical system

$$\frac{d}{dt}\Delta i_{cq} = \Delta i_{cq}\frac{R_c}{L_c} - \Delta i_{cd}\omega + \Delta u_q\frac{1}{L_c} - \Delta v_q\frac{1}{L_c} \tag{14}$$

$$\frac{d}{dt}\Delta i_{cd} = \Delta i_{cq}\omega + \Delta i_{cd}\frac{R_c}{L_c} + \Delta u_d\frac{1}{L_c} - \Delta v_d\frac{1}{L_c} \tag{15}$$

$$\frac{d}{dt}\Delta u_q = -\Delta i_{cq}\frac{1}{C_f} - \Delta u_d\omega + \Delta i_{nq}\frac{1}{C_f} \tag{16}$$

$$\frac{d}{dt}\Delta u_d = -\Delta i_{cd}\frac{1}{C_f} + \Delta u_q\omega + \Delta i_{nd}\frac{1}{C_f} \tag{17}$$

$$\frac{d}{dt}\Delta i_{nq} = -\Delta i_{nq}\frac{R_n}{L_n} - \Delta i_{nd}\omega + \Delta e_q\frac{1}{L_n} - \Delta u_q\frac{1}{L_n} \tag{18}$$

$$\frac{d}{dt}\Delta i_{nd} = +\Delta i_{nq}\omega - \Delta i_{nd}\frac{R_n}{L_n} + \Delta e_d\frac{1}{L_n} - \Delta u_d\frac{1}{L_n} \tag{19}$$

The linearised transforms:

$$\begin{bmatrix}\Delta f_q^c\\ \Delta f_d^c\end{bmatrix} = \begin{bmatrix}1 & 0 & -f_{d0}\\ 0 & 1 & f_{q0}\end{bmatrix}\begin{bmatrix}\Delta f_q\\ \Delta f_d\\ \Delta\theta^c\end{bmatrix} \tag{20}$$

$$\begin{bmatrix}\Delta f_q\\ \Delta f_d\end{bmatrix} = \begin{bmatrix}1 & 0 & f_{d0}\\ 0 & 1 & f_{q0}\end{bmatrix}\begin{bmatrix}\Delta f_q^c\\ \Delta f_d^c\\ \Delta\theta^c\end{bmatrix} \tag{21}$$

The PLL:

$$G_{PLL}(s) = \frac{\Delta\theta^c}{\Delta u_d} = -\frac{K_{p\,pll}s + K_{i\,pll}}{s^2 + K_{p\,pll}u_{q0}s + K_{i\,pll}u_{q0}} \tag{22}$$

The outer loop:

$$\Delta i_{cq}^* = (\Delta P^* - \Delta P)K_P(s) \tag{23}$$

$$\Delta i_{cd}^{'*} = (\Delta U^* - \Delta U)K_U(s) \tag{24}$$

And the current loop:

$$\Delta v_q^c = -(\Delta i_{cq}^* - \Delta i_{cq}^c)\left(K_{p\,cc} + \frac{K_{i\,cc}}{s}\right) - \omega L_c\Delta i_{cd}^c + \Delta u_q^c \tag{25}$$

$$\Delta v_d^c = -(\Delta i_{cd}^* - \Delta i_{cd}^c)\left(K_{p\,cc} + \frac{K_{i\,cc}}{s}\right) + \omega L_c\Delta i_{cq}^c + \Delta u_d^c \tag{26}$$

The linearised PVD:

$$\begin{aligned}\Delta i_{ff} = &-\frac{(X_n^2+R_n^2)i_{cq0}+R_nU}{Z_n\sqrt{U^2-\frac{((X_n^2+R_n^2)i_{cq0}+R_nU)^2}{Z_n^2}}}\Delta i_{cq}^*\\ &\frac{Z_n\left(2U-\frac{2R_n((X_n^2+R_n^2)i_{cq0}+R_nU)}{Z_n^2}\right)}{2\sqrt{U^2\frac{((X_n^2+R_n^2)i_{cq0}+R_nU)^2}{Z_n^2}}} + \frac{X_n^2+R_n^2}{X_c} - X_n\\ &+\frac{}{X_n^2+R_n^2}\Delta U\end{aligned} \tag{27}$$

The linearised converter delay is a 4^{th} order Padé approximation of 1.5 sampling period, resulting in

$$D(s) = \frac{s^4 - 6.67e^5\,s^3 + 2e^9\,s^2 - 3.11e^{14}s + 2.074e^{18}}{s^4 + 6.67e^5\,s^3 + 2e^9\,s^2 + 3.11e^{14}s + 2.074e^{18}} \tag{28}$$

APPENDIX B
PARAMETERS

Parameters	Value
Switching and sampling frequency	5000 Hz
DC Voltage	280 V
Grid voltage (E)	78 V (RMS Ph-N)
Filter resistance (R_c)	0.2 Ω
Filter inductance (L_c)	13 mH
Grid resistance for SCR = 1.38	0.3 Ω
Grid inductance for SCR = 1.38	42 mH
Grid resistance for SCR = 2.77	0.15 Ω
Grid inductance for SCR = 2.77	21 mH
Grid resistance for SCR = 5.53	0.11 Ω
Grid inductance for SCR = 5.53	10.5 mH
Base power	1 kW
Integration period of $\Delta\theta$ ($t_0 \rightarrow t_1$)	−10 ms to 0 ms
Trigger for power reduction ($\Delta\theta_{trigger}$)	20°
Power reduction	50 %
$K_{PLL\,p}$	24.2 rad/(Vs)
$K_{PLL\,i}$	3.22×10^3 rad/(Vs^2)
$K_{CC\,p}$	1.12 V/A
$K_{CC\,i}$	40 V/(As)
$K_{P\,p}$	0.0048 A/W
$K_{P\,i}$	0.35 A/(Ws)
$K_{U\,p}$	−0.0048 A/V
$K_{U\,i}$	−2 A/(Vs)

ACKNOWLEDGMENT

The authors would like to thank Euan Andrew and Dimitrios Vozikis for their hardware and laboratory support. Data Statement: The data used for this study is available at https://doi.org/10.15129/575c3961-619d-42f6-b44e-39cf38c9b185

REFERENCES

[1] UNFCCC, "Adoption of the Paris agreement," Tech. Rep. FCCC/CP 2015/L.9/Rev1, United Nations, 2015. [Online]. Available: https://unfccc.int/resource/docs/2015/cop21/eng/l09r01.pdf

[2] A. Sayigh, D. Milborrow, and J. K. Kaldellis, *The Age of Wind Energy. Innovative Renewable Energy*, Cham, Switzerland: Springer, 2020.

[3] ENTSO-E, "High penetration of power electronic interfaced power sources and the potential contribution of grid forming converters," 2020. [Online]. Available: https://euagenda.eu/upload/publications/untitled-292051-ea.pdf

[4] S. Impram, S. V. Nese, and B. Oral, "Challenges of renewable energy penetration on power system flexibility: A survey," *Energy Strategy Rev.*, vol. 31, Sep. 2018, Art. no. 100539.

[5] O. Anaya-Lara, D. Campos-Gaona, E. Moreno-Goytia, and G. Adam, *Offshore Wind Energy Generation*. Hoboken, NJ, USA: Wiley, 2014.

[6] A. Yazdani and I. Reza, *Voltage Source Converter in Power System*. Hoboken, NJ, USA: Wiley, 2010.

[7] S. Ruihua, Z. Chao, L. Ruomei, and Z. Xiaoxin, "VSCs based HVDC and its control strategy," in *Proc. IEEE/PES Transmiss. Distrib. Conf. Expo.: Asia Pacific*, 2005, pp. 1–6.

[8] M. Davari and Y. A. R. I. Mohamed, "Robust vector control of a very weak-grid-connected voltage-source converter considering the phase-locked loop dynamics," *IEEE Trans. Power Electron.*, vol. 32, no. 2, pp. 977–994, Feb. 2017.

[9] A. Johnson and N. Tleis, "The development of grid code requirements for new and renewable forms of generation in Great Britain," *Wind Eng.*, vol. 29, pp. 201–215, May 2005.

[10] *IEEE Guide for Planning DC Links Terminating At AC Locations Having Low Short-Circuit Capacities*, IEEE Standard 1204-1997, Piscataway, NJ, USA: Institute of Electrical and Electronics Engineers, Jun. 1997. [Online]. Available: https://edisciplinas.usp.br/pluginfile.php/1589095/mod_folder/content/0/IEEE%20Std%201204-1997.pdf?forcedownload=1

[11] S.-J. S. Tsai and K.-H. Wong, "On-line estimation of Thevenin equivalent with varying system states," in *Proc. IEEE Power Energy Soc. Gen. Meeting - Convers. Del. Elect. Energy 21st Century*, 2008, pp. 1–7.

[12] J. Lavenius, L. Vanfretti, and G. N. Taranto, "Performance assessment of PMU-based estimation methods of thevenin equivalents for real-time voltage stability monitoring," in *Proc. IEEE 15th Int. Conf. Environ. Elect. Eng.*, 2015, pp. 1977–1982.

[13] National Grid ESO, "Technical Report on the events of 9 Aug. 2019," Tech. Rep., Sep. 2019. [Online]. Available: https://www.nationalgrideso.com/document/152346/download

[14] K. Givaki, D. Chen, L. Xu, and Y. Xu, "An alternative current-error based control for VSC integration to weak grid," in *Proc. IEEE Power Energy Soc. Gen. Meeting*, 2018, pp. 1–5.
[15] M. F. M. Arani and Y. A. R. I. Mohamed, "Analysis and performance enhancement of vector-controlled VSC in HVDC links connected to very weak grids," *IEEE Trans. Power Syst.*, vol. 32, no. 1, pp. 684–693, Jan. 2017.
[16] X. Chen, Y. Zhang, S. Wang, J. Chen, and C. Gong, "Impedance-phased dynamic control method for grid-connected inverters in a weak grid," *IEEE Trans. Power Electron.*, vol. 32, no. 1, pp. 274–283, Jan. 2017.
[17] D. Yang, X. Ruan, and H. Wu, "Impedance shaping of the grid-connected inverter with LCL filter to improve its adaptability to the weak grid condition," *IEEE Trans. Power Electron.*, vol. 29, no. 11, pp. 5795–5805, Nov. 2014.
[18] J. Z. Zhou, H. Ding, S. Fan, Y. Zhang, and A. M. Gole, "Impact of short-circuit ratio and phase-locked-loop parameters on the small-signal behavior of a VSC-HVDC converter," *IEEE Trans. Power Del.*, vol. 29, no. 5, pp. 2287–2296, Oct. 2014.
[19] H. Khazraj, F. F. D. Silva, and C. L. Bak, "An improved current controller to ensure the robust performance of grid-connected converters under weak grid conditions," in *Proc. Int. Conf. Environ. Elect. Eng.*, 2016, pp. 1–6.
[20] X. Zhang, D. Xia, Z. Fu, G. Wang, and D. Xu, "An improved feedforward control method considering PLL dynamics to improve weak grid stability of grid-connected inverters," *IEEE Trans. Ind. Appl.*, vol. 54, no. 5, pp. 5143–5151, Sep./Oct. 2018.
[21] K. M. Alawasa, Y. A. R. I. Mohamed, and W. Xu, "Active mitigation of subsynchronous interactions between PWM voltage-source converters and power networks," *IEEE Trans. Power Electron.*, vol. 29, no. 1, pp. 121–134, Jan. 2014.
[22] J. Fang, X. Li, H. Li, and Y. Tang, "Stability improvement for three-phase grid-connected converters through impedance reshaping in quadrature-axis," *IEEE Trans. Power Electron.*, vol. 33, no. 10, pp. 8365–8375, Oct. 2018.
[23] A. J. Agbemuko, J. L. Dominguez-Garcia, O. Gomis-Bellmunt, and L. Harnefors, "Passivity-based analysis and performance enhancement of a vector controlled VSC connected to a weak AC grid," *IEEE Trans. Power Del.*, vol. 36, no. 1, pp. 156–167, Feb. 2021.
[24] A. Egea-Alvarez, S. Fekriasl, F. Hassan, and O. Gomis-Bellmunt, "Advanced vector control for voltage source converters connected to weak grids," *IEEE Trans. Power Syst.*, vol. 30, no. 6, pp. 3072–3081, Nov. 2015.
[25] G. Wu, "Analysis and design of vector control for VSC-HVDC connected to weak grids," *CSEE J. Power Energy Syst.*, vol. 3, no. 2, pp. 115–124, Jun. 2017.
[26] J. F. Morris, K. H. Ahmed, and A. Egea-Alvarez, "Analysis of controller bandwidth interactions for vector-controlled VSC connected to very weak AC grids," *IEEE Trans. Emerg. Sel. Topics Power Electron.*, vol. 9, no. 6, pp. 7343–7354, Dec. 2021.
[27] M. Rashed, M. Sumner, A. Ghanem, M. A. Elsayes, and I. I. Mansy, "Grid impedance estimation for islanding detection and adaptive control of converters," *IET Power Electron.*, vol. 10, no. 11, pp. 1279–1288, 2017.
[28] J. Fang, J. Yu, Y. Zhang, and S. M. Goetz, "An estimation-based solution to weak-grid-induced small-signal stability problems of power converters," *IEEE Trans. Emerg. Sel. Topics Power Electron.*, vol. 9, no. 4, pp. 4558–4572, Aug. 2021.
[29] M. Ciobotaru, R. Teodorescu, and F. Blaabjerg, "On-line grid impedance estimation based on harmonic injection for grid-connected PV inverter," in *Proc. IEEE Int. Symp. Ind. Electron.*, 2007, pp. 2437–2442.
[30] M. Cespedes and J. Sun, "Adaptive control of grid-connected inverters based on online grid impedance measurements," *IEEE Trans. Sustain. Energy*, vol. 5, no. 2, pp. 516–523, Apr. 2014.
[31] ö. Göksu, R. Teodorescu, C. L. Bak, F. Iov, and P. C. Kjær, "Instability of wind turbine converters during current injection to low voltage grid faults and PLL frequency based stability solution," *IEEE Trans. Power Syst.*, vol. 29, no. 4, pp. 1683–1691, Jul. 2014.
[32] S. Lu, Z. Xu, L. Xiao, W. Jiang, and X. Bie, "Evaluation and enhancement of control strategies for VSC stations under weak grid strengths," *IEEE Trans. Power Syst.*, vol. 33, no. 2, pp. 1836–1847, Mar. 2018.
[33] J. Khazaei, P. Idowu, A. Asrari, A. B. Shafaye, and L. Piyasinghe, "Review of HVDC control in weak AC grids," *Electric Power Syst. Res.*, vol. 162, pp. 194–206, 2018.
[34] M. Ashabani and Y. A.-R. I. Mohamed, "Integrating VSCs to weak grids by nonlinear power damping controller with self-synchronization capability," *IEEE Trans. Power Syst.*, vol. 29, no. 2, pp. 805–814, Mar. 2014.
[35] L. Wang, ed., *Modeling and Control of Sustainable Power Systems: Towards Smarter and Greener Electric Grids*, (Green Energy and Technology Series). Berlin Heidelberg:Springer2011.
[36] M. K. D. Meerendre, E. Prieto-Araujo, K. H. Ahmed, O. Gomis-Bellmunt, L. Xu, and A. Egea, "Review of local network impedance estimation techniques," *IEEE Access*, vol. 8, pp. 213647–213661, 2020.
[37] A. V. Timbus, R. Teodorescu, F. Blaabjerg, and U. Borup, "Online grid measurement and ENS detection for PV inverter running on highly inductive grid," *IEEE Power Electron. Lett.*, vol. 2, no. 3, pp. 77–82, Sep. 2004.
[38] J. Kukkola, M. Routimo, and M. Hinkkanen, "Real-time grid impedance estimation using a converter," in *Proc. IEEE Energy Convers. Congr. Expo.*, 2019, pp. 6005–6012.
[39] N. P. W. Strachan and D. Jovcic, "Stability of a variable-speed permanent magnet wind generator with weak AC grids," *IEEE Trans. Power Del.*, vol. 25, no. 4, pp. 2779–2788, Oct. 2010.
[40] L. Zhang, "Modeling and control of VSC-HVDC links connected to weak AC systems," Ph.D. dissertation, KTH Royal Institute of Technology, Stockholm, Sweden, 2010.
[41] P. Kundur, *Power System Stability and Control*. New York, NY, USA: McGraw-Hill, 1993.
[42] R. Bugdał, A. Dyśko, G. M. Burt, and J. R. Mcdonald, "Performance analysis of the ROCOF and vector shift methods using a dynamic protection modelling approach," in *Proc. 15th Int. Conf. Power Syst. Protection*, 2006, pp. 139–144.

MATHIEU KERVYN DE MEERENDRE received the M.Eng. degree from the University of Bath, Bath, U.K., in 2014. Before starting his Ph.D., he worked on various aerospace and subsea projects in industry. In 2017, he joined the Wind and Marine Energy Systems Centre of Doctoral Training, University of Strathclyde, Glasgow, U.K. His research focuses on renewable energy integration with a focus on converters and control.

KHALED H. AHMED (Senior Member, IEEE) received the B.Sc. (Hons.) and M.Sc. degrees from Alexandria University, Alexandria, Egypt, in 2002 and 2004, respectively, and the Ph.D. degree in power electronics applications from the University of Strathclyde, Glasgow, U.K., 2008. Since 2019, he has been a Professor with Alexandria University. He is currenetly a Reader in power electronics with the University of Strathclyde. He has authored or coauthored more than 100 technical papers in refereed journals and conferences as well as a published textbook entitled *High Voltage Direct Current Transmission: Converters, Systems and DC Grids*, a book chapter contribution, and a PCT patent PCT/GB2017/051364. His research interests are renewable energy integration, high power converters, offshore wind energy, DC/DC converters, HVDC, and smart grids. He is a Senior Member of the IEEE Power Electronics and Industrial Electronics societies.

AGUSTÍ EGEA-ÀLVAREZ (Member, IEEE) received the B.Sc., M.Sc., and Ph.D. degrees from the Technical University of Catalonia, Barcelona, Spain, in 2008, 2010 and 2014 respectively. In 2015, he was a Marie Curie Fellow with the China Electric Power Research Institute. In 2016, he joined Siemens Gamesa as a Converter Control Engineer working on grid forming controllers and alternative HVDC schemes for offshore wind farms. He is a Strathclyde Chancellors Fellow (Lecturer) with the Electronic & Electrical Engineering Department and has been a member of the PEDEC (Power Electronics, Drives and Energy Conversion) Group since 2018.

His research interests include control and operation of high-voltage direct current systems, renewable generation systems, electrical machines and power converter control. He is a Member of IET and has been involved in several CIGRE and ENTSOE working groups.